DrEngMuslim - Karya Ilmiah - Comparing Natural And Synthetic Polymeric Nanofluids In A Mid-Permeability Sandstone Reservoir Condition

by Drengmuslim Karya Ilmiah

Submission date: 19-Aug-2022 08:11AM (UTC+0700)
Submission ID: 1884147969
File name: nofluids_in_a_mid-permeability_sandstone_reservoir_condition.pdf (3.79M)
Word count: 8903
Character count: 47544

ResearchGate

See discussions, stats, and author profiles for this publication at: https://www.researchgate.net/publication/343379587

Comparing natural and synthetic polymeric nanofluids in a mid-permeability sandstone reservoir condition

Article *in* Journal of Molecular Liquids · August 2020

DOI: 10.1016/j.molliq.2020.113947

CITATIONS
7

READS
149

10 authors, including:

Agi Augustine
Universiti Teknologi Malaysia
71 PUBLICATIONS **949** CITATIONS

SEE PROFILE

Radzuan Junin
Universiti Teknologi Malaysia
176 PUBLICATIONS **2,430** CITATIONS

SEE PROFILE

Afeez Olayinka Gbadamosi
Universiti Teknologi Malaysia
62 PUBLICATIONS **1,026** CITATIONS

SEE PROFILE

Mohammad A. Manan
Universiti Teknologi Malaysia
50 PUBLICATIONS **1,194** CITATIONS

SEE PROFILE

Some of the authors of this publication are also working on these related projects:

Project
A study of biodiesel from waste cooking oil catalyzed by Sarawak novel ostrich-eggshell based catalyst (2016 - 2019) (now looking for a Graduate Research Assistant (GRA)) View project

Project
Waxy crude oils flow behavior View project

All content following this page was uploaded by Radzuan Junin on 29 April 2021.

The user has requested enhancement of the downloaded file.

Journal of Molecular Liquids 317 (2020) 113947

Contents lists available at ScienceDirect

Journal of Molecular Liquids

journal homepage: www.elsevier.com/locate/molliq

Comparing natural and synthetic polymeric nanofluids in a mid-permeability sandstone reservoir condition

Augustine Agi [a,b], Radzuan Junin [a,b,*], Afeez Gbadamosi [a,c], Muhammad Manan [a], Mohd Zaidi Jaafar [a,b,*], Mohammed Omar Abdullah [d], Agus Arsad [b], Nur Bashirah Azli [a], Muslim Abdurrahman [e], Faruk Yakasai [a,f]

[a] Department of Petroleum Engineering, School of Chemical and Energy Engineering, Faculty of Engineering, Universiti Teknologi Malaysia, 81310 Johor Bahru, Malaysia
[b] Drilling and Production Enhanced Research Group, UTM MPRC-Institute for Oil and Gas, Universiti Teknologi Malaysia, 81310 Johor Bahru, Malaysia
[c] Department of Chemical and Petroleum Engineering, College of Engineering, Afe Babalola University, PMB 5454 Ado-Ekiti, Nigeria
[d] Department of Chemical Engineering and Energy Sustainability, Faculty of Engineering, Universiti Malaysia Sarawak, Kota Samarahan, Sarawak, Malaysia
[e] Department of Petroleum Engineering, Universitas Islam Riau, Jl. Kaharudin Nasution, No. 113 KM 11, Perhentian Marpoyan, Pekanbaru, 28284, Riau, Indonesia
[f] Department of Chemical and Petroleum Engineering, Faculty of Engineering, Bayero University, Kano PMB3011, Nigeria

ARTICLE INFO

Article history:
Received 12 April 2020
Received in revised form 5 July 2020
Accepted 28 July 2020
Available online 1 August 2020

Keywords:
Biopolymer
Polymeric nanofluids
Starch nanoparticles
Thermal degradation
EOR

ABSTRACT

Biopolymeric nanofluids have been proposed as an eco-friendly substitute to synthetic polymeric nanofluids to cut cost and environmental effect. However, previous studies on the use of biopolymeric nanofluids to enhance oil recovery focused only on adsorption and fluid injectivity at ambient condition. In this study, the thermal degradation of crystalline starch nanofluid (CSNF) at reservoir condition was investigated and compared with silica and aluminium oxide polymeric nanofluids, SiO_2PNF and Al_2O_3PNF respectively. The thermal degradation of the polymeric nanofluids was investigated using Brookfield RST rheometer. Moreover, interfacial tension (IFT) properties and wettability alteration efficiency of the polymeric nanofluids were determined using Easy Dyne KRUSS tensiometer and sessile drop technique, respectively. Finally, the oil displacement ability of the polymeric nanofluids at typical reservoir condition was studied using Fars EOR technologies high-pressure high-temperature apparatus. Experimental result shows that the viscosities of SiO_2PNF and Al_2O_3PNF decreased with increase in temperature, whereas the viscosity of CSNF increased with temperature. Besides, CSNF exhibited a significant decrease in IFT at all conditions investigated while IFT results of SiO_2PNF and Al_2O_3PNF showed a non-monotonic trend with increase in temperature. Moreover, CSNF showed better potential to alter wettability at all conditions. The microscopic image of the emulsion generated shows stability of the emulsion over a long period and confirmed the ability of CSNF to withstand high temperature degradation compared to SiO_2PNF and Al_2O_3PNF. Finally, it was observed that the mobility ratio of water flooding approaches unity faster than that of SiO_2PNF, Al_2O_3PNF and CSNF, respectively. It can be concluded from this study that 13–23% incremental oil recovery can be achieved with the use of polymeric nanofluids.

© 2020 Published by Elsevier B.V.

1. Introduction

The low production from existing reservoirs and less discoveries of new fields has posed a real problem to the oil and gas industries. About 50–70% original oil in place (OOIP) are still trapped in the reservoir after initial recovery and water flooding [1]. Enhanced oil recovery (EOR) methods are one of the viable options that can reduce the gap between demand and supply. EOR processes are used to improve the productivity of the fields which aims to recover the oil left in the reservoirs.

Over the years numerous EOR methods such as gas, thermal and chemical (alkali, surfactants, and polymers) have been used to overcome the low oil sweep efficiency [2]. Chemical EOR (CEOR) technique is deemed highly favourable due to its better proficiency, reasonable capital cost, practical and financial possibilities. EOR chemicals such as alkali and surfactants can reduce interfacial tension (IFT) by altering rock/fluid interface in the reservoir. They can also alter wettability between oil-water (O/W) interface [3]. Polymer flooding is the widely applied CEOR technique to increase viscosity and control mobility. Field results have shown that it can recover up to 5–30% OOIP [4].

Hydrolysed polyacrylamide (HPAM) is a widely used polymer in flooding, because of inexpensive handling cost, relatively resistant to bacterial attack, high solubility in water and high ability to reduce permeability of water [5,6]. However, with variation in crude oil properties and harsh environmental conditions of the reservoir, current chemical

* Corresponding authors at: Department of Petroleum Engineering, School of Chemical and Energy Engineering, Faculty of Engineering, Universiti Teknologi Malaysia, 81310 Johor Bahru, Malaysia.
E-mail addresses: r-radzuan@utm.my (R. Junin), mzaidi@utm.my (M.Z. Jaafar).

https://doi.org/10.1016/j.molliq.2020.113947
0167-7322/© 2020 Published by Elsevier B.V.

flooding materials have limitations such as degradation and precipitation. Therefore, various studies are being carried out to improve the limitations of polymers such as HPAM against high temperature and high salinity reservoir conditions. More recently, researchers have reported the use of nanofluid in CEOR process. Nanofluid which is the synergy of base fluid with nanoparticles has the advantages of being more tolerant to high salinity, high temperature, longer stability, less plugging and retention in highly permeable reservoir [7].

The recent trend in nanotechnology has focused on incorporating polymers with nanoparticles to produce fluids with distinct characteristics from the polymers and nanoparticles [8]. Various studies have reported the use of silica (SiO_2) [9–11]; titanium dioxide (TiO_2) [12]; graphene oxide (GO) [13]; and aluminium oxide (Al_2O_3) [5] nanoparticles to improve the viscosity, degradation, salinity, and viscoelastic properties of HPAM. They reported that the presence of nanoparticles significantly improved the properties of HPAM against environmental factors. Despite the extensive investigation from previous research for EOR application, there are still some challenges on its field application owing to cost, transport and retention in reservoir might pose huge environmental problems [14,15]. Nanoparticles from renewable materials have been sought after to replace inorganic and metallic nanoparticles. The large-scale availability of starches, cellulose and fibres that are known to have long chain polysaccharides to withstand harsh reservoir conditions and their broad applicability has attracted researchers. Starch nanoparticles have found success in pharmaceutical, confectionary, cosmetics, food industry and more importantly EOR.

Wei et al. [15] and Molnes et al. [16] have reported the use of cellulose nanoparticles and crystalline cellulose nanoparticles respectively as displacement fluids in EOR. The cellulose nanofluid were stable and well dispersed in 2.0 wt% of electrolyte and the oil displacement in a micromodel showed that the cellulose nanofluid enhanced the sweep efficiency and decreased residual oil saturation [15]. The flooding experiments show that the cellulose nanocrystals have good injectivity and the rheological properties show stable and long propagation through the core [16]. However, in the study by Molnes et al. [16], sandstone cores were used whereas Wei et al. [15] reported the use of sand-pack and a micromodel in their study. Sand-packs and micromodels are only representative of reservoir cores, as they cannot provide the real heterogeneity of a reservoir. Furthermore, while the procedure for preparing micromodel, glass beads and sand-packs is proper, it does not consider the likelihood of fluid propagation through the sidewalls. Fines movement and fluid channelling through sidewalls occur in a sand-pack/micromodel flooding test and are not considered, despite having significant influence on the flooding result. Overall, both studies failed to consider the effect of temperature in the flooding process, the thermal degradation of the biopolymeric nanofluids in porous media and the mechanisms of EOR.

For us to come to a logical conclusion in the search for a high performance EOR chemical, there is need to compare the efficiency of biopolymeric nanofluids with their inorganic and metallic polymeric nanofluid counterparts at the same conditions. Therefore, in this study the thermal degradation of crystalline starch nanofluid (CSNF) was compared with SiO_2 polymeric nanofluid (SiO_2PNF) and Al_2O_3 polymeric nanofluid (Al_2O_3PNF). The IFT properties of CSNF at oil-water interface and wettability alteration efficiency of CSNF were compared with SiO_2PNF and Al_2O_3PNF at the same conditions. The oil recovery performance of the polymeric nanofluids was compared at typical reservoir conditions (temperature of 120 °C, pressure of 3000 psi and salinity of 22,000 ppm).

2. Materials and methods

2.1. Materials

HPAM with degree of hydrolysis 25 mol%, mol/wt of 20×10^6 Da was acquired from SNF Floerger, Paris. SiO_2 (inorganic nanoparticles) with a purity of 99.5%, 15–20 nm size and mol/wt 60.8 g/mol was obtained from US Research nanomaterial Inc. USA. Al_2O_3 (metallic nanoparticles) with a purity of 99%, 20 nm size and mol/wt 101.96 g/mol was obtained from Sky Springs Nanomaterials Inc., Houston, TX, USA. CSNP (biopolymeric nanoparticles) with purity >99%, size of 6.97–163 nm was produced from native cassava starch with amylopectin (75 wt%) and amylose (25 wt%) as described by Agi et al. [17,18]. Sodium chloride (NaCl) with 99% purity and mol/wt 58.44 g/mol was obtained from Merck group. An intermediate crude oil from an oilfield in Sarawak, Malaysia (density of 0.8283 g/mL @25 °C, API gravity 37.7 and viscosity of 10 mPa.s @25 °C) was used for the experiments. Three mid-permeability sandstone cores from the same outcrop were utilized for the contact angle and core flooding tests. The physical properties of the sandstone cores are shown in Table 1. The X-ray diffraction (XRD) of the core (Fig. 1) reveals that the samples are mainly quartz (98.9%) and illite (1.1%).

2.2. Methods

2.2.1. Polymeric nanofluids preparation

SiO_2PNF and Al_2O_3PNF were made by a two-stage technique. A 0.1 wt% each of SiO_2 and Al_2O_3 were dispersed in deionized water (DIW) and sonicated for 35 min to form a homogenous dispersion. HPAM (0.1 wt%) was added to the nanofluids dispersion and agitated for 23 h on a stirrer. On the other hand, 0.2 wt% of CSNP was dissolved in DIW, stirred for 6 h and ultrasonicated for 1 h. To investigate the effect of salinity on the polymeric nanofluids, NaCl with different concentrations (0.9–2.2 wt%) was added to the polymeric nanofluid suspension and stirred for 24 h. The salinity range depicts a typical Malay Basin salinity [19].

2.2.2. Characterization of polymeric nanofluids

To determine the microstructures and morphology of the nanoparticles, a transmission electron microscopy (TEM) HITACHI (HT 7700) image analyser was used. Samples were captured at electrical energy of 120 kV. An inbuilt HITACHI EMIP-SP electron microscope image integration software automatically measured the particles sizes and enhanced the images. Shimadzu IR Tracer-100 Fourier transform infrared (FTIR) was utilized to determine the functional groups of CSNP and interaction between SiO_2PNF and Al_2O_3PNF within a scanning range of 500 to 4000 cm^{-1}. A light scattering instrument (Anton Paar Litesizer™ 500) was used to determine stability and surface charge of the polymeric nanofluids. The polymeric nanofluids (0.1 wt%) were dissolved in distilled water (DW) and transferred to omega cuvette for analysis. The analysis was carried out at a back-scattering angle of 170° at 25 °C. The refractive index of water was 1.3303 and the viscosity of water was 0.8903 mPa.s.

2.2.3. Rheological analysis

The rheology of SiO_2PNF, Al_2O_3PNF and CSNF were determined using Brookfield RST rheometer. The rheometer is composed of temperature control connected to water bath for high temperature conditions. All the measurements were carried out at 1–1000 s^{-1} (shear rate) at a temperature range of 26–80 °C. For repeatability, the experiments were conducted in triplicate and the average reported.

Table 1
Properties of sandstone core.

Diameter (cm)	Length (cm)	Bulk Volume (cm^3)	Pore Volume (cm^3)	Porosity (%)	Permeability (mD)
3.7	9.8	100.37	17.00	16.9	201

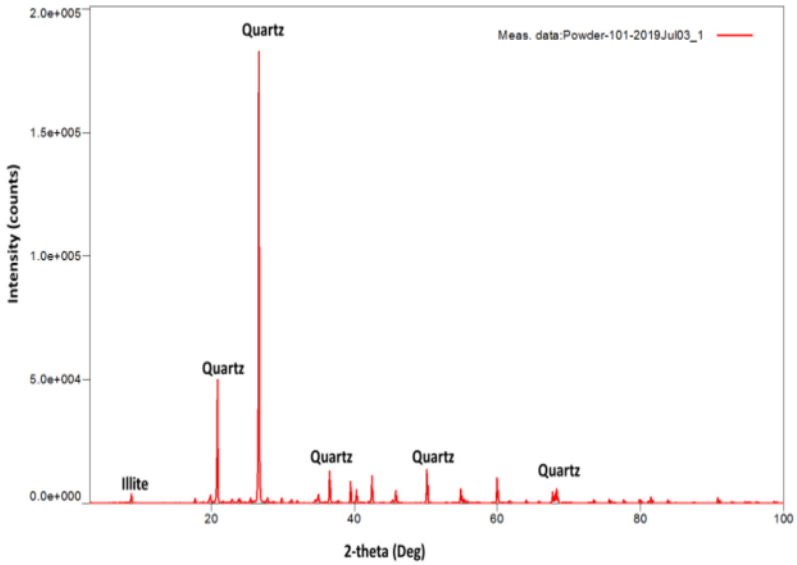

Fig. 1. XRD pattern of sandstone core.

2.2.4. IFT determination

The IFT between SiO_2PNF, Al_2O_3PNF, CSNF and oil were determined with Easy Dyne tensiometer (K20) by Kruss GmbH, Germany. It was connected to a water-bath to control temperature of the tensiometer. IFT of polymeric nanofluids at different concentration (0.05–0.2 wt%) as a function of NaCl concentrations (0.9–2.2 wt%) and temperature (26–80 °C) were determined.

2.2.5. Core samples preparation and wettability determination

Core samples of 1 cm thick and 5 cm in diameter with a flat surface were used for the contact angle determination. The cores were washed with DW and toluene to get rid of impurities, and dried for 24 h. The samples were placed in a beaker and rendered oil-wet by pipetting oil samples on the surface until it was completely immersed in crude oil. The beaker was sealed to prevent evaporation and contamination, and placed in the oven for 78 h at 90 °C. To evaluate the wettability alteration efficiency of SiO_2 PNF, Al_2O_3 PNF and CSNF under static condition, the cores were treated with 0.2 wt% of the polymeric nanofluids for 78 h and dried for 24 h. Wettability alteration before and after treatment with polymeric nanofluids were estimated by determining the contact angles. It was achieved by using a curved needle to place a drop of oil on a horizontally held core as shown in Fig. 2. The images of the drops (26–80 °C) were captured with a digital camera and analysed with image analyser software (Image J 1.48 s) to determine the contact angles.

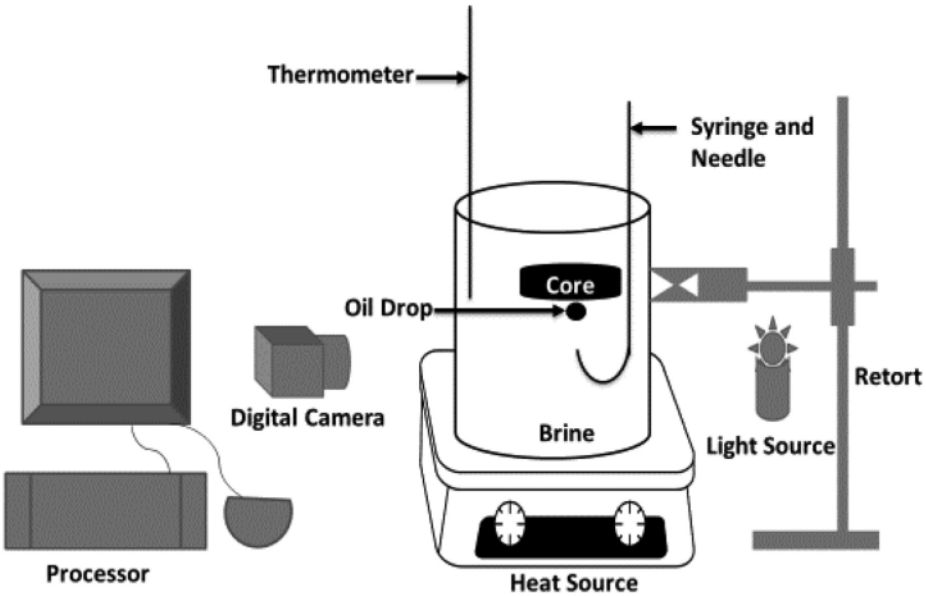

Fig. 2. Experimental setup used for wettability test.

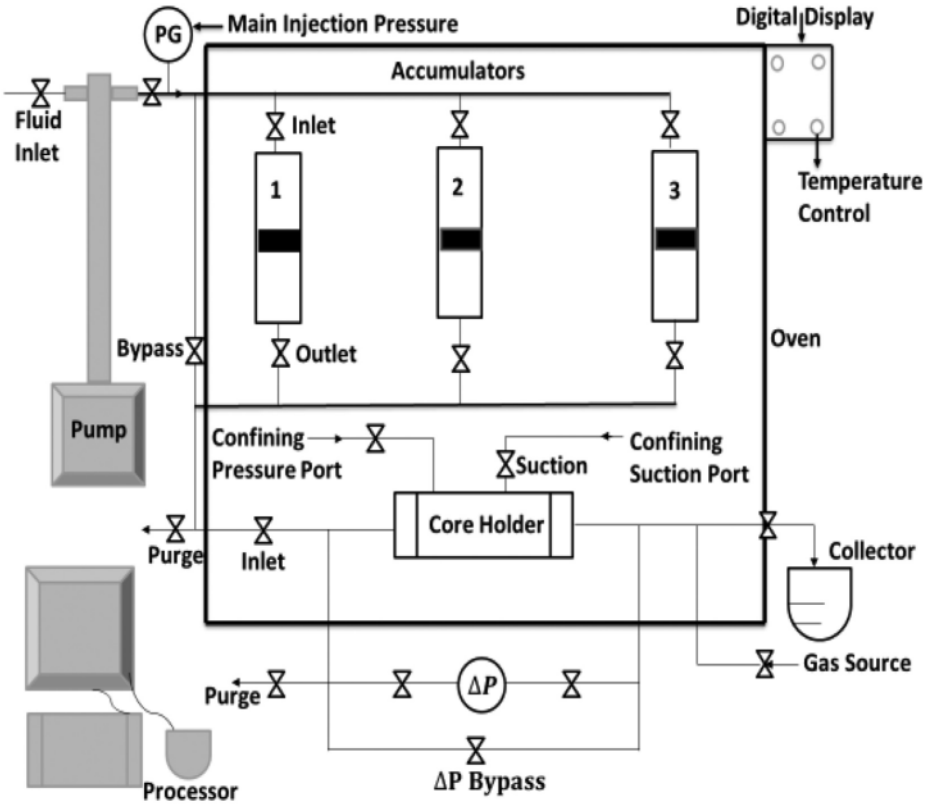

Fig. 3. Schematic representation of core-flood equipment.

2.2.6. Core flooding test

The core flooding was investigated using a high-pressure high-temperature (HPHT) apparatus manufactured by Fars EOR technologies (Fig. 3). The equipment consists of a furnace for temperature regulation, four accumulators for injecting fluid and a compartment for holding the core. It has a temperature limit of 150 °C and pressure capacity of 6000 psi. Three identical mid-permeability core samples from the same outcrop as that utilized for the contact angle test were utilized

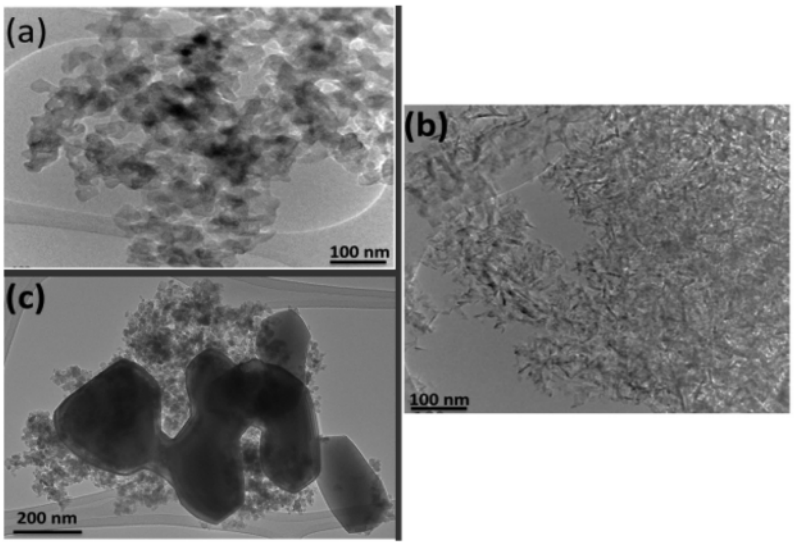

Fig. 4. TEM image of (a) SiO_2 nanoparticles, (b) Al_2O_3 nanoparticles, and (c) CSNP.

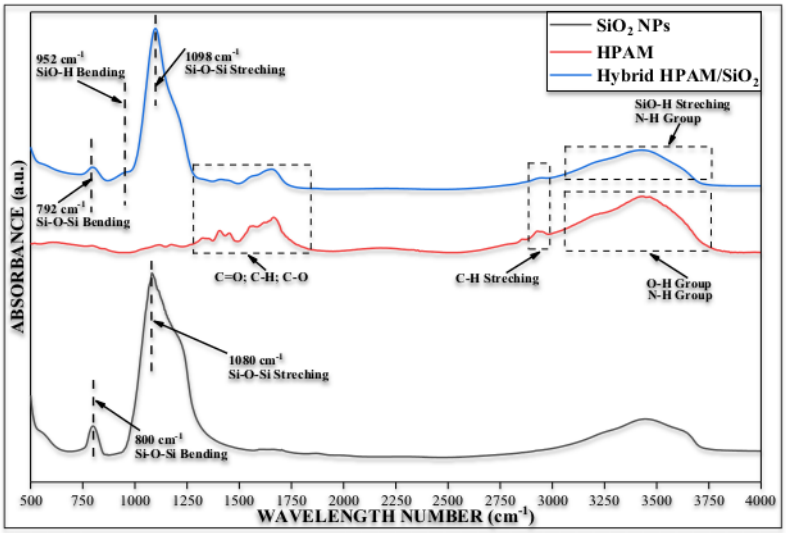

Fig. 5. FTIR spectra of SiO_2PNF.

for oil displacement test (Table 1). Core samples were washed with toluene in a Soxhlet distillation extractor column before and after each use, the cores were subsequently dried for 24 h at 95 °C in an oven. Oil displacement tests were executed to determine the oil recovery efficiency of SiO_2 PNF, Al_2O_3 PNF and CPNF. To simulate the reservoir condition of a typical Sarawak oilfield, the equipment was pressured to 3000 psi, supported with a back pressure (100 psi) and oven temperature raised to 120 °C. After vacuuming, the system was saturated with 2.2 wt% of synthetic brine and flooded with oil until connate water was achieved. ISCO pump was utilized in pumping injectants from accumulators to the equipment. Crude oil was introduced into the core at 0.5 mL/min and aged for 24 h to achieve equilibrium. Consequently, water was injected at a constant flow rate until breakthrough occurred. Then, 0.5 PV consisting of 0.2 wt% of different polymeric nanofluids were injected to recover the bypassed oil. Chase water (0.5 PV) was later injected to recover any remaining oil. All the experiments were conducted in duplicate and the average reported.

3. Results and discussion

3.1. Polymeric nanofluids characterization

TEM images of SiO_2, Al_2O_3 and CSNP are shown in Fig. 4. It shows that SiO_2 nanoparticles has a semi-crystalline structure with spherical shape, with sizes ranges from 15 to 20 nm (Fig. 4a). Fig. 4b shows that Al_2O_3 nanoparticles has irregular, spiral shape with size of about 20 nm. On the other hand, CSNP shows spherical crystalline particles of size range 10.1–19.1 nm. The grains formed platy and pear-like shapes (Fig. 4c) of around 163 nm from which smaller particles emerged.

FTIR analysis of the polymeric nanofluids is presented as Figs. 5, 6 and 7. The result of SiO_2PNF in comparison with pure SiO_2 nanoparticles and HPAM are shown in Fig. 5. SiO_2PNF showed two peaks at 1098 cm^{-1} and 792 cm^{-1} representing the vibration of Si-O-Si unit. The crest at 962 cm^{-1} shows the vibration of Si-OH, which was created by the

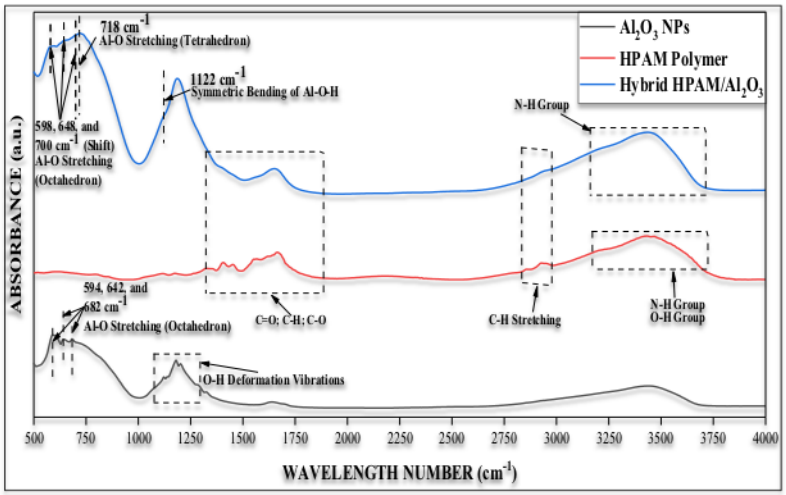

Fig. 6. FTIR spectra of Al_2O_3PNF.

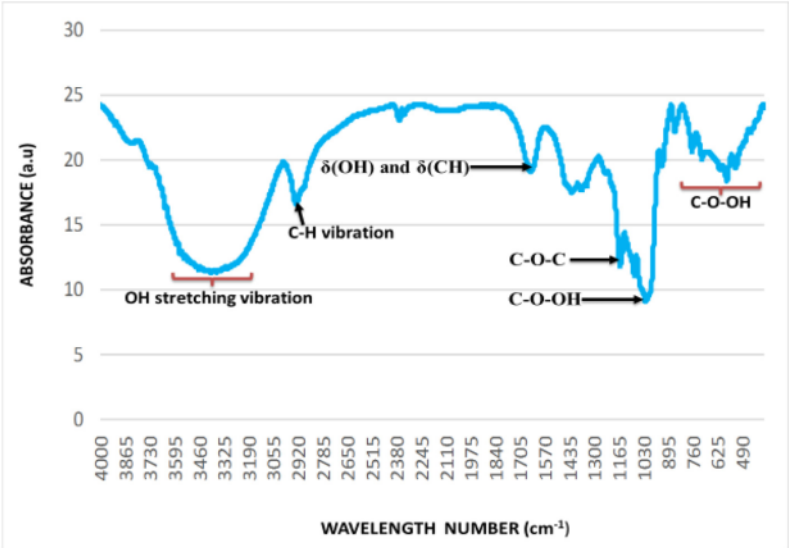

Fig. 7. FTIR spectra of CSNP.

-OH unit on the surface of SiO_2. The OH groups reacted with -COOH, -CHO and -NH_2 on the HPAM to form SiO – H···NH or SiO – H···O – CNH_2 or SiO…HNH – CO – C (strong hydrogen bridges and hydrolysable covalent crosslinks). Whereas the bands at 1350, 1500, and 1650 cm^{-1} correspond to Si—O, Si-NH_2, and -NH_2, respectively. Broad peak at 3100–3750 cm^{-1} indicates N—H, -OH, and Si-OH vibration, this interaction between HPAM and SiO_2 nanoparticles resulted to a hybrid SiO_2PNF [11].

Fig. 6 displays the FTIR spectra of Al_2O_3PNF in comparison with Al_2O_3 nanoparticles and HPAM. The peaks at 718 and 1122 cm^{-1} correspond to tetrahedral shape Al—O and the vibration of Al-O-H which was necessitated by -OH band on the alumina surface. The vibration of the carboxyl unit of HPAM appeared at 1652 cm^{-1}. Also, Al—O – H…N – H or Al—O – H…O – $CHNH_2$ shows a strong hydrogen link among the -OH unit on Al_2O_3 and oxygen/nitrogen of the amide group present in the HPAM. The hydrogen units in the HPAM and the oxygen unit in the Al_2O_3 formed Al-O…HNH – CO – C hydrogen bonds. This led to a strong hydrolysable crosslink in the Al_2O_3PNF [5].

CSNP showed a broad peak between 3500 and 3200 cm^{-1} which represent the stretching vibration of OH group of the cellulose present (Fig. 7). The peak at 2930 cm^{-1} is characteristic of C—H vibration, whereas the crest at 1650 cm^{-1} represents δ(OH) and δ(CH) adsorption of water. Peak at 1650 cm^{-1} corresponds to the C=O band of the carboxyl and carbonyl groups. The stretching vibration C-O-C was observed at 1158 cm^{-1}. The D-glycopyran group, C—O and attached OH was observed between 1080 and 709 cm^{-1}.

Colloidal stability of polymeric nanofluids dispersion can be envisaged by the magnitude of the zeta potential. To determine the stability of the polymeric nanofluids, the zeta potential with time was determined. The results (Fig. 8) show negligible variation in the values of the zeta potential with time and the error bar shows that the uncertainty is minimal which confirms the repeatability of the experiments. Moreover, the polymeric nanofluid was still stable as no rapid coagulation or flocculation was observed. This could be because of the repulsive interaction or electrostatic forces between the suspended particles that impeded the aggregation and agglomeration of the particles thereby rendering it stable [20]. The slight shift in the zeta potential result is due to the difference in the location of the slipping plane of the polymeric nanofluids and the presence of disassociated carboxylic groups [21–23]. The negative value of the Al_2O_3PNF confirms the success of the surface coating with HPAM. CSNF showed higher surface charge compared to SiO_2PNF and Al_2O_3PNF. This could be attributed to microfluidization of the CSNP, which led to the higher zeta potential [18]. It might also be due to the replacement of the hydroxyl group by the sulfate ester group (-OSO_3^-) during synthesis of CSNP that produced an electrostatic repulsion. Therefore, it can be concluded that the presence of these randomly distributed negative charge surface ester groups on the surface of CSNP and the disassociation of the remaining valences contributed to the high zeta potential which contributed to its stability.

3.2. Comparison of the rheology of polymeric nanofluids

The flow performance of SiO_2PNF, Al_2O_3PNF and CSNF at the same concentration (0.2 wt%) were compared. All the polymeric nanofluids exhibited pseudoplastic and shear thinning at high and low shear rates (Fig. 9). This might be due to strong electrostatic hydrogen linkage between silanol group and the HPAM, and the covalent linkages of the aluminol functional group and HPAM amino group [5,6]. However, the viscosity of CSNF was greater than SiO_2PNF and Al_2O_3 at the same concentration. It might be because of the electroviscous negative charge on the surface of the CSNP and the formation of a stronger particle-particle

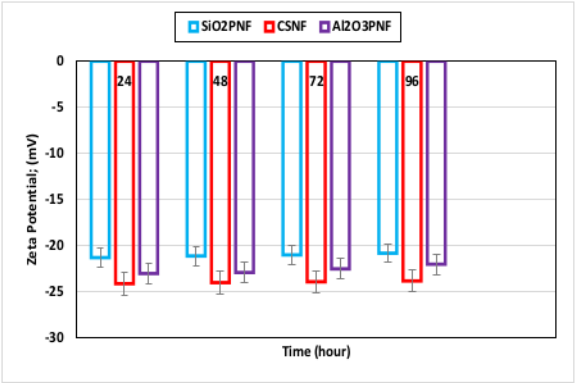

Fig. 8. Zeta potential of polymeric nanofluids.

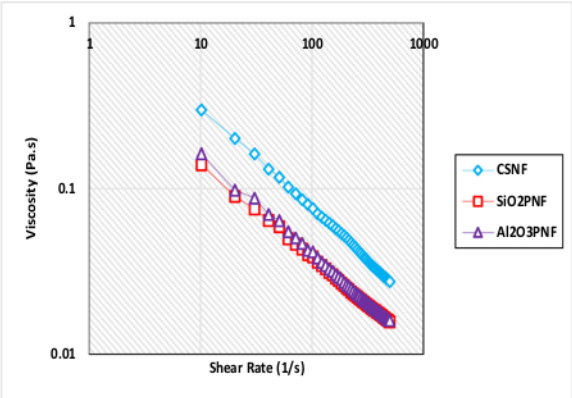

Fig. 9. Apparent viscosity of polymeric nanofluids.

hydrogen bonds compared to that formed by silanol and aluminol group on HPAM. The result is coherent with previous work of Shafiei-Sabet et al. [24]. They reported that the rheological properties of cellulose nanocrystals vary due to their surface charge and ionic strength.

3.3. Impact of salinity on viscosity of polymeric nanofluids

Reservoir brine poses a serious problem on flow behaviour of injected EOR fluids. Therefore, a comparative study on the salinity resistance of SiO_2PNF, Al_2O_3PNF and CSNF were investigated. The results (Fig. 10) show that the viscosity of the polymeric nanofluids reduced as concentration of NaCl increased. Which might be because of screening effect of Na^+ which reduced the repulsive energy of the polymeric nanofluids and the hydrodynamic volumes of the polymeric nanofluid subsequently reducing viscosity [18,25]. All the polymeric nanofluids still retained their pseudoplastic and shear-thinning behaviour as salinity increases. This behaviour can be likened to the uniformity of the polymeric nanofluids as shear rate increases, as initially agglomerated nanoparticles begins to separate [26]. But the effect of salinity was mild for CSNF compared to SiO_2 and Al_2O_3. This is because of the electric double layer (EDL) and reduction in Debye's length of CSNF compared to SiO_2PNF and Al_2O_3PNF. EDL force are repulsive in nature therefore, they decreased the agglomeration of the CSNP and hence the stability of the CSNF [20]. This was necessitated by the higher collision among the CSNP which affected the presence of the salt [27].

3.4. Thermal degradation of polymeric nanofluids

The thermal degradation of a material is very important when determining the energy needed to overpower the activation energy of flow as material moves from one equilibrium to another. Fig. 11 shows the effect of temperature (26–80 °C) on the viscosity of the polymeric nanofluids at the same concentration (0.2 wt%). The results show that the viscosities of the polymeric nanofluids are dependent on temperature. The viscosities of SiO_2PNF and Al_2O_3PNF declined as temperature increased [28]. This is because decrease in adsorption of HPAM on SiO_2 and Al_2O_3 nanoparticles. As temperature increases, there is dihydroxylation of hydrogen bond on the silanol and aluminol group that weakened the structure of the SiO_2PNF and Al_2O_3PNF which might have induced a hydrophobic nature and resulted in the decrease in viscosity [4]. The viscosity of Al_2O_3PNF was higher compared to SiO_2PNF. This is because of the formation of COO^- group during hydrolysis of HPAM at high temperature, which necessitated the continuous adsorption of HPAM on Al_2O_3 due to the electrostatic interaction of Al^{3+} and COO^-. Whereas there was no interaction between the negatively charged SiO_2. The CSNF showed a reversed trend in comparison with SiO_2PNF and Al_2O_3PNF, as the temperature increases the viscosity increased. This could be because of increase in tensile strength due to binding of the CSNF which might have initiated a strong cohesive bond between the CSNP [29]. It might also be due to the formation of a three-dimensional (micelle type) network of flocs after the synthesis of CSNP that resulted in the increase of viscosity. Furthermore, heating induces the melting CSNP crystal into their composing molecules which might have resulted to increase in viscosity [30,31]. Also, heating might have caused expansion and disruption of inter and intra molecular hydrogen bond in the CSNP and increased the starch-water hydrogen bond. Consequently, the increase in temperature of the CSNF facilitated swelling of the CSNP [27]. Owing to the fact that during the acidolysis process only the non-crystalline area of the starch was destroyed, the crystalline area was preserved, which basically keeps the same crystal structure as that of the native starch. This is consistent with earlier work of Xiao et al. [32] where they reported that the inter and intra molecular hydrogen bond of native starch breaks with increase in temperature and the crystal structure disappears resulting in a sharp rise in viscosity. The result shows that even at high temperature the interaction between the CSNP still exist which demonstrated the thermal stability of CSNP when it is propagated through oil field reservoirs. The uncertainty of the experimental results (Figs. 10 and 11) is shown by the error bar which indicates that the uncertainty is rather small, and the difference is not significant.

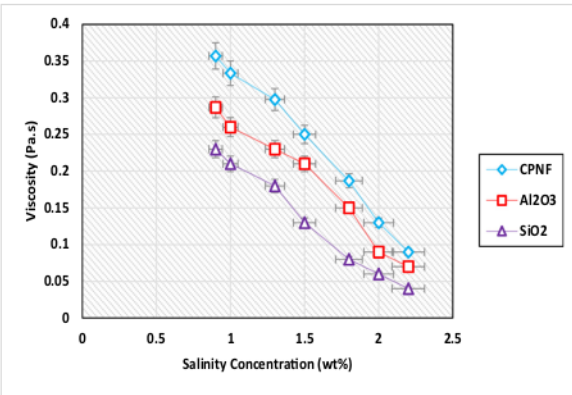

Fig. 10. Effect of salinity on the apparent viscosity of polymeric nanofluids.

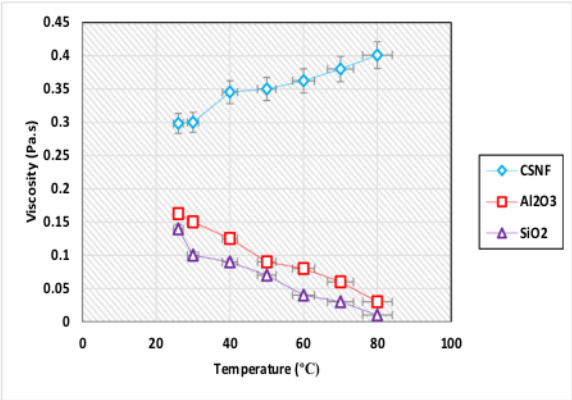

Fig. 11. Effect of temperature on polymeric nanofluids.

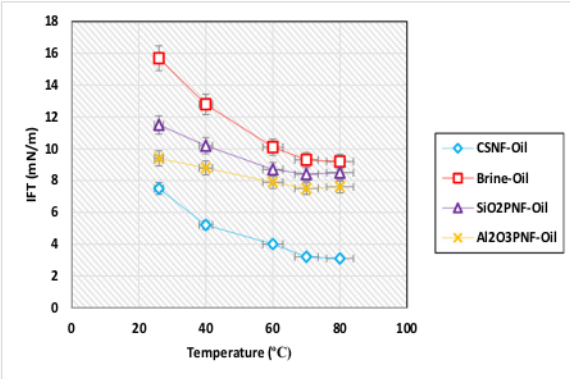

Fig. 12. IFT of polymeric nanofluid in the presence of brine (2.2 wt%) as a function of temperature.

3.5. Impact of polymeric nanofluids on IFT

IFT between trapped oil and displacing fluid plays a significant role in oil recovery. Reducing IFT decreases severity at the interface and allows deformation of the O/W interface, which leads to improved oil recovery. Nanofluids have been reported to reduce IFT. The interfacial properties strongly hinges on the quality of surface-active agent which moves to the interface of O/W. Besides, the movement of this surface-active agent from bulk to the interface depends on the medium temperature. Therefore, the influence of temperature (26–80 °C) on adsorption of surface-active agents formed from SiO_2PNF, Al_2O_3PNF and CSNF at the interface of oil and brine (2.2 wt%) were studied. Fig. 12 shows the IFT of SiO_2PNF, Al_2O_3PNF and CSNF compared to brine as a function of temperature, with standard error bar almost the same. This signifies certainty that the mean computed value estimated the true mean value of the experimental results. The results show that there is a significant decrease in IFT in the presence of polymeric nanofluids compared to brine alone. It could be credited to the electrostatic interaction of the polymeric nanofluids and brine in the bulk, which increases the dispersion of the polymeric nanofluids to the interface of O/W [33]. The interaction between the polymeric nanofluids in the presence of brine was found to be lower than that of brine alone (Fig. 12). This singularly confirms the formation surface-active agent from electrostatic attraction between polymeric nanofluids and brine which could have significantly reduce O/W IFT compared to brine alone. Therefore, it can be concluded that impact of electrostatic attraction is foremost over the effect of electrostatic repulsion in decreasing IFT.

As the temperature of the polymeric nanofluid increases, the liquid molecules had higher kinetic energy, there was a rapid migration of polymeric nanofluid from the bulk to the O/W interface. This can be attributed to thermophoresis phenomenon of the nanofluids which migrated the particles from a region of high temperature (hot zone) to a region with lower temperature (cold zone) [20,34]. This led to a significant adsorption of the polymeric nanofluid at the interface resulting in a charged EDL which decreased the coating at the interface. The arrangement of the polymeric nanofluids at the interface will increase the number of impurities, but in brine the impurities are salted off [35]. This weakens the cohesive energy and expands the intermolecular energies at the interface thereby reducing IFT of the polymeric nanofluids.

However, IFT of SiO_2PNF and Al_2O_3PNF at the interface of O/W showed a non-monotonic tendency as temperature increased. It was observed that IFT of SiO_2PNF and Al_2O_3PNF decreased to 8.4 ± 0.25 mN/m and 7.5 ± 0.22 mN/m respectively as the temperature was increased to 70 °C. A further increase in temperature (80 °C) of the system increased the IFT. This is because as the temperature increases, it promotes the detachment of the HPAM from the nanoparticles and promotes only the migration/adsorption of the nanoparticles at the interface (Fig. 13). As temperature increases SiO_2PNF and Al_2O_3PNF begin to desorb from the interface because of thermal instabilities. This indicates that at higher temperature, there were increased chances of aggregation and consequently a decreased activity at the interface

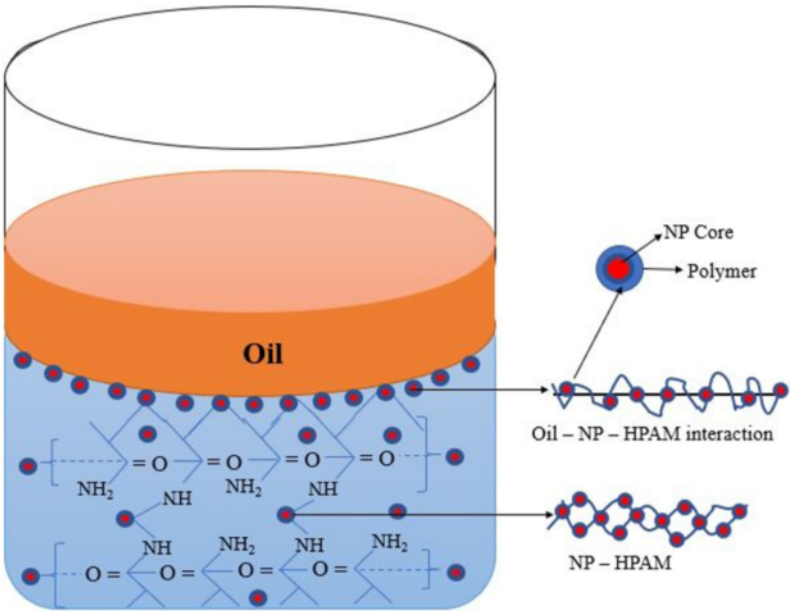

Fig. 13. Mechanism of IFT reduction in the presence of SiO_2PNF and Al_2O_3PNF.

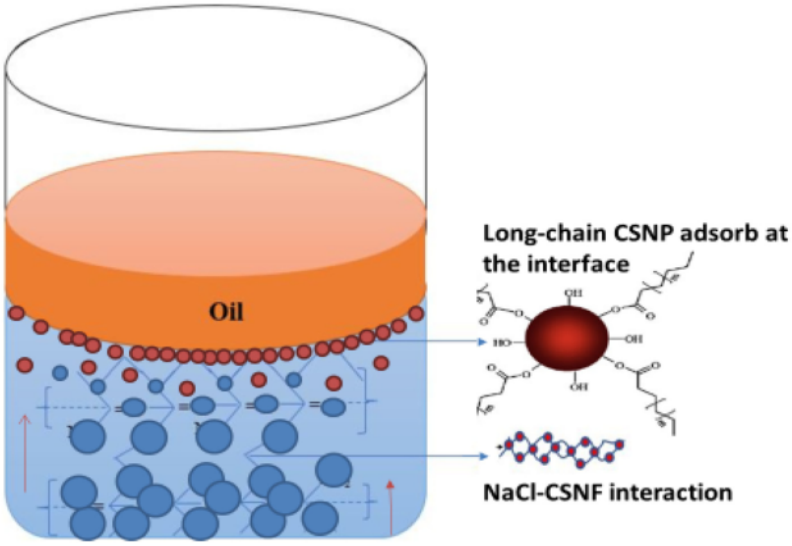

Fig. 14. Mechanism of IFT reduction in the presence of CSNF.

[36]. This is coherent with prior work of Gbadamosi et al. [6]. They also observed a sudden increase in IFT, which implies that the surface-active agent at the interface has diminished due to desorption.

The IFT of CSNF continued to decrease even at higher temperature of 80 °C and it showed the lowest IFT at all temperatures (Fig. 12). This might be due to the breakage of larger droplet to smaller ones as temperature increases (cavitation) and the increase in hydrophobicity of the CSNF [25,37]. Temperature increased the free energy per unit surface area at the interface for CSNF compared to SiO_2PNF and Al_2O_3PNF [33]. The result is consistent with rheology result (Fig. 11) as increase in temperature created a three-dimensional network that increased the viscosity. The long chain CSNP arranged themselves at the interface (Fig. 14) hindering the development of anisotropic phase in the CSNF and induced the creation of EDL which reduced the layer of interface and IFT.

3.6. Impact of polymeric nanofluids on wettability alteration

Wettability controls displacement of wetting and non-wetting phase of fluid at pore-scale. As such a change in the wettability from oil-wet to water-wet can enhance fluid flow. However, reservoir salinity can affect the stability of injected fluid and temperature can affect the wetting of solid surface. It is, therefore, important to investigate the impact of salinity and temperature on different polymeric nano-modified sandstone surfaces. To achieve this, the influence of SiO_2PNF, Al_2O_3PNF and CSNF (0.2 wt%) on the wettability alteration of oil-wet sandstone at reservoir salinity (2.2 wt%) and different temperatures (26–80 °C) were investigated. The results show the reference angles of the sandstone core to be 114 and 144 degrees (Fig. 15).

The wettability of oil wet cores was altered to water-wet when treated with polymeric nanofluids (Fig. 15). This might be because of polymeric nanofluid adsorption on sandstone surface that altered wettability. This is because of the disassociation of the two atoms of Na and Cl to form Na^+ and Cl^- ions. The quartz in the sandstone core (Fig. 1) attracts Na^+ to form a layer on sandstone core, the high concentration of NaCl (2.2 wt%) means excess of positive Na^+ ions on the sandstone surface to attract the negative parts of polar components present in crude oil. However, the monovalent ions of Na^+ covering the sandstone core prevented contact between crude oil and sandstone core. As a result of this interaction, the film present on the sandstone core surface was not disrupted by bases or acids in the crude oil. Therefore, this might be the main reason which might have altered the wettability.

The reduction of contact angle as temperature increases confirms stability of nanofluids when it is propagation in porous medium. Temperature reduces the number of active sites on the sandstone core which might have influenced the spreading behaviour of the polymeric nanofluids [25]. The dispersion of the polymeric nanofluids front increases as temperature increased, temperature break-down the bonds and water molecules desolvated the polymeric nanofluids, this might have increased the attraction of the sandstone surface to the polymeric nanofluids [38]. Furthermore, the heat and mass transfer of the nanoparticles might have been enhanced due to the micro-conventional and mechanical agitation induced by Brownian motion of the polymeric nanofluids [20,34]. Also, temperature decreases asphaltenes precipitation which is washed out from the sandstone surface by the adsorbing polymeric nanofluids. The nanoparticles could make asphaltene suspended in the oil and rapidly adsorb them thereby inhibiting them from being precipitated [39]. This is coherent with earlier findings of Akbarzadeh et al. [40] and Escrochi et al. [41]. They stated that above the bubble point pressure, more asphaltene is in liquid phase therefore

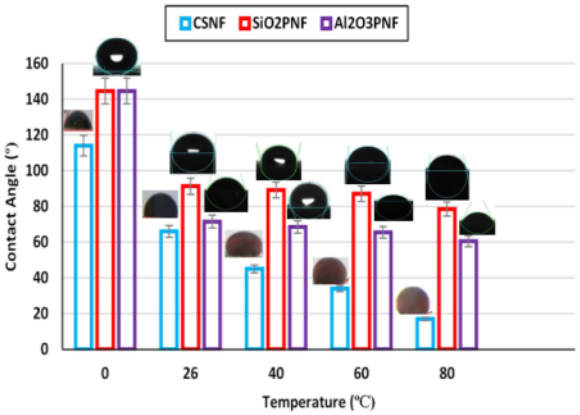

Fig. 15. Oil contact angles and microscopic image of oil drops at different temperatures.

for a saturated and single-phase reservoir, increases in temperature will increases asphaltene solubility so its precipitation decreases, and the reservoir become water wet. CSNF showed better potential to alter wettability compared to SiO_2PNF and Al_2O_3PNF at all conditions. This could be attributed to a better electrostatic attraction and high affinity of CSNF to adsorb on sandstone surface. It might also be due to steric force which led to adsorption of the organic molecules on the sandstone surface [20]. It can therefore be concluded from this study that SiO_2PNF and Al_2O_3PNF had a lower adsorption on sandstone surface which resulted to a low reduction in contact angle. The standard error of the contact angle and temperature were determined for three tests. The error bars were used to determine the positive and negative standard error from the mean of the contact angle and temperature. It was observed from the error bar (Fig. 15) that the results show good parallelism, indicating that the experimental results are reliable.

3.7. Oil displacement results

To determine the efficiency, effective treatment methods and the potentials of the polymeric nanofluids for EOR, series of core flooding experiments were performed to mimic water flooding and polymeric nanofluid flooding of a Sarawak oil field. The difference in cumulative oil recovery in the secondary and tertiary recovery modes are presented in Fig. 16. Water flooding recovered 48% OOIP, which signifies that sufficient quantity of oil was bypassed. Tertiary recovery was initiated, and oil recovery increased by 13%, 17% and 23% with SiO_2PNF, Al2O$_3$PNF and CSNF, respectively. This is because the polymeric nanofluid blocked the permeable channels created by water flooding and recovered additional oil from small pores [42]. The reduction in IFT between the O/W facilitated the mobilization of the initially bypassed oil. The results are consistent with IFT and wettability result, which decreased as temperature increased. It therefore shows that the polymeric nanofluid were still stable at high salinity (2.2 wt%) and HPHT (3000 psi, 120 °C) reservoir conditions.

The pressure drop profile shows a good relationship with recovery result (Fig. 17). When waterflood commenced, there was a rise in pressure drops, followed by a decline until it became constant. The reason for the declining trend is due to the high mobility of water compared to oil, which was evident as breakthrough time saw the pressure drop remain constant. A favourable type of displacement will occur if

$$\frac{k_{rw}\mu_w}{k_{ro}\mu_o} = M \leq 1 \quad (1)$$

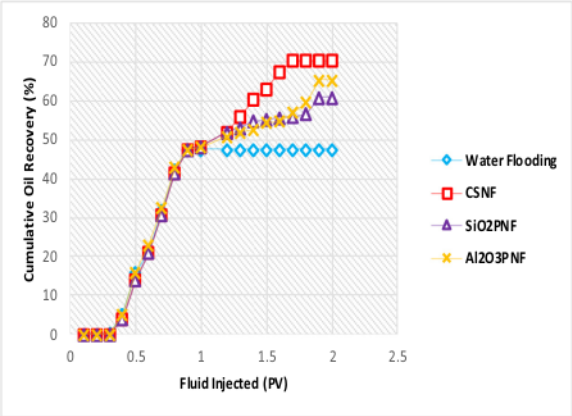

Fig. 16. Cumulative oil recovery of polymeric nanofluids.

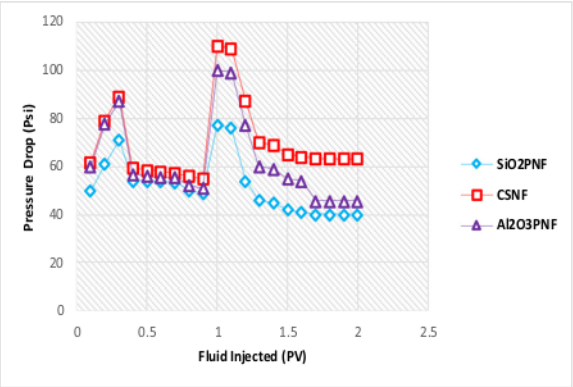

Fig. 17. Pressure drop of polymeric nanofluids.

whereas, M is mobility ratio, μ_o is viscosity of oil (mPa.s), μ_w is viscosity of water (mPa.s), k_{ro} and k_{rw} are end point relative permeabilities of oil and water respectively (mD). Mobility ratio was determined using the method of Bamidele et al. [43] and it was observed that the mobility ratio of water flooding approaches unity faster than that of SiO_2PNF, Al_2O_3PNF and CSNF (Fig. 18). This might have resulted in by-passing of oil and consequently early breakthrough in the water flooding, which is consistent with pressure drop profile (Fig. 17). The delay in approaching unity for SiO_2PNF, Al_2O_3PNF and CSNF signifies that the oil viscosity variation is less than their viscosity variation resulting in a favourable mobility. EOR also saw an increase in the profile, the rise during tertiary recovery is due to their improved viscosity compared to water [42].

Increase in pressure drop as polymeric nanofluid were introduced also demonstrated that the polymeric nanofluids lowered the capillary forces holding the oil in pore spaces [44,45]. The pressure drops remained very high even at elevated temperature which confirms that the polymeric nanofluids were still stable and oil displacement efficiency was still very active at 120 °C, which resulted to increased oil recovery. As the nanofluids imbibe into the sandstone core to expel trapped oil, the pressure profile began to build leading to the formation of O/W emulsion (Fig. 19). This agrees with earlier work of Pei et al. [46] who stated that O/W emulsion enhanced the sweep efficiency by blocking the channel created by water and lowered the oil mobility.

The emulsion generated was examined with an Amscope microscope (Fig. 20). Emulsions generated by SiO_2PNF and Al_2O_3PNF (Fig. 20a and b respectively) showed large drops sizes with high-level

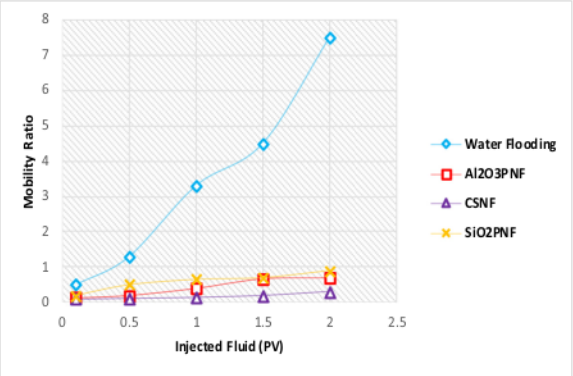

Fig. 18. Mobility ratio of polymeric nanofluids.

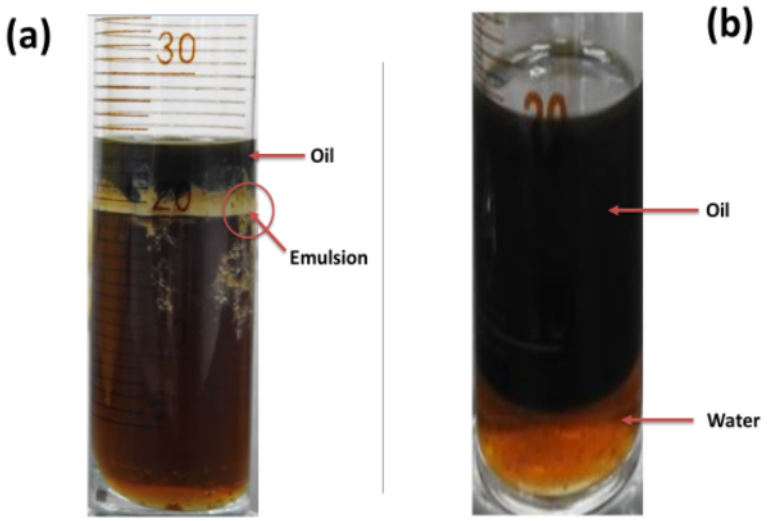

Fig. 19. Emulsion generated during (a) polymeric nanofluid flooding (b) water flooding.

of coalescence compared to CSNF emulsion (Fig. 20c) which has small diameter droplets which signifies stability of the emulsion over a long period, which is consistent with the zeta potential result with time (Fig. 8). This agrees with the recovery results as this singular phenomenon might be one of the reasons for the higher recovery of CSNF compared to SiO_2PNF and Al_2O_3PNF. The result also confirmed the ability of CSNF to withstand high temperature degradation compared to SiO_2PNF and Al_2O_3PNF, which is consistent with the thermal degradation results (Fig. 11). This agrees with prior work by Hatscher [47] who stated that at a temperature of 135 °C, the viscosity of biopolymer schizophyllan was still stable and the stability lasted for 300 days under anaerobic conditions. The biopolymer also exhibited superb laboratory and field pilot test results in comparison with xanthan and sulfonated polyacrylamide.

4. Conclusions

The present study is focused on comparing the EOR mechanisms and oil displacement behaviour of inorganic, metallic, and bio-polymeric nanofluids which are promising for EOR applications. The morphology of the nanoparticles was determined using TEM, whereas FTIR was used to determine the functional group and interaction between the polymeric nanofluids. Also, the stability of the polymeric nanofluids with time was determined by zeta potential. The thermal degradation and EOR mechanisms of the polymeric nanofluids were compared and related to the oil displacement ability of the polymeric nanofluids. Based on the experimental results the following conclusions were reached.

1. The surface chemistry of polymeric nanofluids shows possible interaction with other EOR materials and zeta potential results show stability of the polymeric nanofluids.
2. The results show that the viscosities of the polymeric nanofluids are dependent on temperature. The viscosities of SiO_2PNF and Al_2O_3PNF decreased with increase in temperature whereas the viscosity of CSNF increased with increase in temperature.
3. The polymeric nanofluids show good potential in decreasing IFT. Meanwhile, the IFT of SiO_2PNF and Al_2O_3PNF showed a non-monotonic trend with increases in temperature.
4. CSNF showed better potential to alter wettability compared to SiO_2PNF and Al_2O_3PNF at all conditions.
5. A range of 13–23% incremental oil recovery was achieved with the use of polymeric nanofluid. The microscopic image of the emulsion generated shows stability of the emulsion over a long period and confirmed the ability of CSNF to withstand high temperature degradation compared to SiO_2PNF and Al_2O_3PNF. The study suggests that the CSNF could be used as an appropriate substitute to conventional CEOR materials.

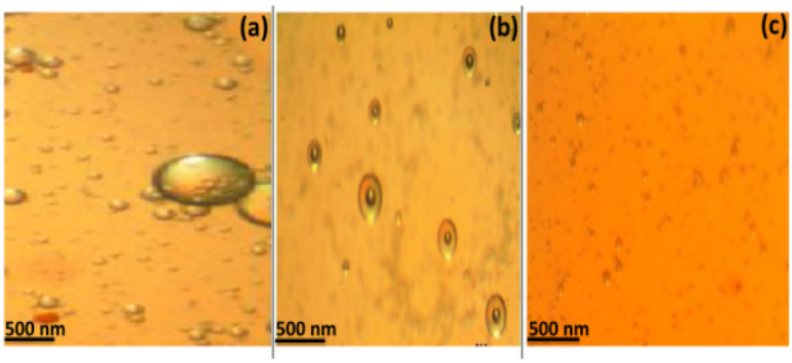

Fig. 20. Microscopic image of emulsion generated during (a) SiO_2PNF flooding, (b) Al_2O_3PNF flooding, and (c) CSNF flooding.

CRediT authorship contribution statement

Augustine Agi: Conceptualization, Methodology, Formal analysis, Investigation, Data curation, Writing - original draft, Visualization. **Radzuan Junin:** Conceptualization, Methodology, Validation, Resources, Visualization, Supervision, Funding acquisition. **Afeez Gbadamosi:** Conceptualization, Formal analysis, Investigation, Data curation. **Muhammad Manan:** Methodology, Validation, Resources, Visualization, Supervision. **Mohd Zaidi Jaafar:** Methodology, Validation, Resources, Visualization, Supervision, Funding acquisition. **Mohammed Omar Abdullah:** Methodology, Validation, Resources, Visualization, Supervision. **Agus Arsad:** Methodology, Validation, Resources, Supervision, Funding acquisition. **Nur Bashirah Azli:** Software, Investigation, Resources, Project administration. **Muslim Abdurrahman:** Methodology, Formal analysis, Resources. **Faruk Yakasai:** Software, Data curation.

Declaration of competing interest

The authors have no conflict of interest.

Acknowledgements

The authors would like to thank the Ministry of Higher Education, Malaysia and Universiti Teknologi Malaysia for supporting this research through Research Management Grants Vot. No. R.J130000.3551.07G52&06G69, R.J130000.2451.08G93, R.J 130000.3051.01M99, and R.J 130000.7351.4B545.

References

[1] A.O. Gbadamosi, J. Kiwalabye, R. Junin, A. Augustine, A review of gas enhanced oil recovery schemes used in the North Sea, Journal of Petroleum Exploration and Production Technology 8 (4) (2018) 1373–1387.
[2] A.O. Gbadamosi, R. Junin, M.A. Manan, A. Agi, A.S. Yusuff, An overview of chemical enhanced oil recovery: recent advances and prospects, International Nano Letters (2019) 1–32.
[3] A. Abbas, A. Moslemizadeh, W.R. Sulaiman, M.Z. Jaafar, A. Agi, An insight into di-chain surfactant adsorption onto sandstone minerals under different salinity-temperature conditions: chemical EOR applications, Chem. Eng. Res. Des. 153 (2020) 657–665.
[4] G.A. Pope, Recent developments and remaining challenges of enhanced oil recovery, J. Pet. Technol. 63 (07) (2011) 65–68.
[5] A. Gbadamosi, R. Junin, M. Manan, A. Agi, J. Oseh, J. Usman, Synergistic application of aluminium oxide nanoparticles and oilfield polyacrylamide for enhanced oil recovery, J. Pet. Sci. Eng. 182 (2019), 106345.
[6] A. Gbadamosi, R. Junin, M. Manan, A. Agi, J. Oseh, J. Usman, Effect of aluminium oxide nanoparticles on oilfield polyacrylamide: rheology, interfacial tension, wettability and oil displacement studies, J. Mol. Liq. 296 (2019), 111863.
[7] A. Agi, R. Junin, A. Gbadamosi, Tailoring of nanoparticles for chemical enhanced oil recovery, International Journal of Nanomanufacturing 16 (2) (2020) 107–147.
[8] A.O. Gbadamosi, R. Junin, M.A. Manan, A. Agi, J. Oseh, Nanotechnology Application in Chemical Enhanced Oil Recovery: Current Opinion and Recent Advances, IntechOpen, 2019 1–20.
[9] A. Maghzi, A. Mohebbi, R. Kharrat, M.H. Ghazanfari, An experimental investigation of silica nanoparticles effect on the rheological behavior of polyacrylamide solution to enhance heavy oil recovery, Pet. Sci. Technol. 31 (2013) 500–508.
[10] N. Lai, X. Guo, N. Zhou, Q. Xu, Shear resistance properties of modified nanoSiO2/AA/AM copolymer oil displacement agent, Energies 9 (2016) 1037.
[11] Z. Hu, M. Haruna, H. Gao, E. Nourafkan, D. Wen, Rheological properties of partially hydrolyzed polyacrylamide seeded by nanoparticles, Ind. Eng. Chem. Res. 56 (2017) 3456–3463.
[12] A.O. Gbadamosi, R. Junin, M.A. Manan, N. Yekeen, A. Augustine, Hybrid suspension of polymer and nanoparticles for enhanced oil recovery, Polym. Bull. 76 (12) (2019) 6193–6230.
[13] M.A. Haruna, S. Pervaiz, Z. Hu, E. Nourafkan, D. Wen, Improved rheology and high-temperature stability of hydrolyzed polyacrylamide using graphene oxide nanosheet, J. Appl. Polym. Sci. 47582 (2019) 1–13.
[14] A. Agi, R. Junin, A. Gbadamosi, Mechanism governing nanoparticles flow behaviour in porous media: insight for enhanced oil recovery applications, Int Nano Lett 8 (2) (2018) 49–77.
[15] B. Wei, Q. Li, J. Ning, Y. Wang, L. Sun, W. Pu, Macro and micro scale observation of a surface functionalized nanocellulose based on aqueous nanofluid in chemical enhanced oil recovery (C-EOR), Fuel 236 (2019) 1321–1333.
[16] S.N. Molnes, I.P. Torrijos, S. Strand, K.G. Paso, K. Syverud, Sandstone injectivity and salt stability of cellulose nanocrystals (CNC) dispersions—premises for use of CNC in enhanced oil recovery, Ind. Crop. Prod. 93 (2016) 152–160.
[17] A. Agi, R. Junin, A. Gbadamosi, A. Abbas, N.B. Azli, J. Oseh, Influence of nanoprecipitation on crystalline starch nanoparticle formed by ultrasonic assisted weak-acid hydrolysis of cassava starch and the rheology of their solutions, Chemical Engineering and Processing-Process Intensification 142 (2019), 107556.
[18] A. Agi, R. Junin, A. Arsad, A. Abbas, A. Gbadamosi, N.B. Azli, J. Oseh, Ultrasonic-assisted weak-acid hydrolysis of crystalline starch nanoparticles for chemical enhanced oil recovery, Int. J. Biol. Macromol. 148 (2020) 1251–1271.
[19] A. Agi, R. Junin, A.Y.M. Alqatta, A. Gbadamosi, A. Yahya, A. Abbas, Ultrasonic ultrafiltration process for the emulsification of oil field produced water treatment, Ultrason. Sonochem. 51 (2019) 214–222.
[20] O. Mahian, L. Kolsi, M. Amani, P. Estelle, G. Ahmadi, C. Kleinstreuer, J.S. Marshall, M. Siavashi, R.A. Taylor, H. Niazmand, S. Wongwises, T. Hayat, A. Kolanjiyil, A. Kasaeian, I. Pop, Recent advances in modeling and simulation of nanofluid flows-part I: fundamentals and theory, Phys. Rep. 790 (2019) 1–48.
[21] S. Chibowski, E.O. Mazur, J. Patkowski, Influence of ionic strength on the adsorption properties of the system dispersed aluminium oxide-polyacrylic acid, Mater. Chem. Phys. 93 (2005) 262–271.
[22] A.E. Wiacek, Influence of dipalmitoylphosphatidylcholine (or dioleoylphosphatidylcholine) and phospholipase A2 enzyme on the properties of emulsions, Journal of Colloids and Interface Science 373 (2012) 75–83.
[23] L.M. Corredor, M.M. Husein, B.B. Maini, Effect of hydrophobic and hydrophilic metal oxide nanoparticles on the performance of xanthan gum solutions for heavy oil recovery, Nanomaterials 9 (94) (2019) 1–13.
[24] S. Shafiei-Sabet, W.Y. Hamad, S. Hatzikiriakos, Rheology of nano-crystalline cellulose aqueous suspensions, Langmuir 28 (49) (2012) 17124–171333.
[25] A. Agi, R. Junin, A. Abbas, A. Gbadamosi, N.B. Azli, Effect of dynamic spreading and the disperse phase of crystalline starch nanoparticles in enhancing oil recovery at reservoir condition of a typical Sarawak oil field, Appl. Nanosci. 10 (1) (2020) 263–279.
[26] W. Samutsri, M. Suphantharika, Effect of salt on pasting, thermal and rheological properties of rice starch in the presence of non-ionic and ionic hydrocolloids, Carbohydr. Polym. 87 (2012) 1559–1568.
[27] A.M. Shi, D. Li, L. Wang, B. Adhikari, Suspension of vacuum-freeze dried starch nanoparticles: influence of NaCl on their rheological properties, Carbohydr. Polym. 94 (2013) 782–790.
[28] L. Qiu, N. Zhu, Y. Feng, E.E. Michaelides, G. Zyla, D. Jing, X. Zhang, P.M. Norris, C.N. Markides, O. Mahian, A review of recent advances in thermophysical properties at the nanoscale: from solid state to colloids, Phys. Rep. 843 (2020) 1–81.
[29] F.E. Eichie, A.E. Amalime, Evaluation of the binder effects of the gum of mucilages of Cissus populnea and Acassia senegal on the mechanical properties of paracetamol tablets, Afr. J. Biotechnol. 6 (19) (2007) 2208–2211.
[30] H.Y. Kim, S.S. Park, S.T. Lim, Preparation, characterization, and utilization of starch nanoparticles, Colloids Surf. B: Biointerfaces 126 (2015) 607–620.
[31] M.P. Herrera, T. Vasanthan, L. Chen, Rheology of starch nanoparticles as influenced by particle size, concentration and temperature, Food Hydrocoll. 66 (2017) 237–245.
[32] H. Xiao, F. Yang, Q. Lin, Q. Zhang, L. Zhang, S. Sun, W. Han, G. Liu, Preparation and characterization of broken-rice starch nanoparticles with different sizes, Int. J. Biol. Macromol. 160 (2020) 437–445.
[33] N. Yekeen, E. Padmanabhan, A.K. Idris, Synergetic effect of nanoparticles and surfactant on n-decane-water interfacial tension and bulk foam stability at high temperature, J. Pet. Sci. Eng. 179 (2019) 814–830.
[34] L. Yang, W. Ji, M. Mao, J. Huang, An updated review on the properties, fabrication and application of hybrid-nanofluids along with their environmental effects, J. Clean. Prod. 257 (2020), 120408.
[35] A. Bera, A. Mandal, B. Guha, Synergic effect of surfactant and salt mixture on interfacial tension reduction between crude oil and water in enhanced oil recovery, J. Chem. Eng. Data 59 (1) (2014) 89–96.
[36] S.F. Sofla, M. Abbasian, M. Mirzaei, Synthesis and micellar characterization of novel pH-sensitive thiol-ended triblock copolymer via combination of RAFT and ROP processes, International Journal of Polymeric Materials and Polymeric Biomaterial 68 (6) (2019) 297–307.
[37] S. Gaikwad, A. Pandit, Ultrasound emulsification: effect of ultrasound and physiochemical properties on dispersed phase volume and droplet size, Ultrason. Sonochem. 15 (2008) 554–563.
[38] S. Strand, E.J. Hognesen, T. Austad, Wettability alteration of carbonates-effects of potential determining ions (Ca2+ and SO42-) and temperature, Coll. Surf. A. Physicochem. Eng. Asp. 275 (2006) 1–10.
[39] Y. Kazemzadeh, S. Eshranghi, K. Kazemi, S. Sourani, M. Mehrabi, Y. Ahmadi, Behavior of asphaltene adsorption onto the metal oxide nanoparticles surface and its effect on the heavy oil recovery, Ind. Eng. Chem. Res. 54 (1) (2015) 233–239.
[40] K. Akarzadeh, O. Sabbagh, J. Beck, W.Y. Svrcek, H.W. Yarranton, Asphaltene precipitation from bitumen diluted with n-alkanes, Paper PETSOC-2004-026-EA, Presented at Canadian International Petroleum Conference Held in Calgary, Alberta June 2004, pp. 8–14.
[41] M. Escrochi, M. Nabipour, S. Ayatollahi, N. Mehranbod, Wettability alteration at elevated temperature: consequences of asphaltene precipitation, Paper SPE-112428-MS, Presented at SPE International Symposium and Exhibition on Formation Damage Control Held in Lafayette, Louisiana, USA, 13-15 February 2008.
[42] N. Kumar, A. Mandal, Surfactant stabilized oil-in-water nanoemulsion: stability, interfacial tension and rheology study for enhanced oil recovery application, Energy Fuel 32 (6) (2018) 6452–6466.

[43] A. Bamidele, A. Fadairo, A. Falode, Endpoint mobility ratios for vertical and horizontal wells with incidence of scale deposition, The Open Petroleum Engineering Journal 2 (2009) 17–23.
[44] M. Dong, S. Ma, Q. Liu, Enhanced heavy oil recovery through interfacial instability: a study of chemical flooding for Brintnell heavy oil, Fuel 88 (2009) 1049–1056.
[45] A. Agi, R. Junin, M.A. Abdullah, M.Z. Jaafar, A. Arsad, W.R. Wan Sulaiman, M.N.A. Mohd Norddin, M. Abdurrahman, A. Abbas, A. Gbadamosi, N.B. Azli, Application of polymeric nanofluid in enhancing oil recovery at reservoir condition, J. Pet. Sci. Eng. 194 (2020) 107476.
[46] H. Pei, G. Zhang, J. Ge, I. Jin, C. Ma, Potential of alkaline flooding to enhance heavy oil recovery through water-in oil emulsion, Fuel 104 (2013) 272–278.
[47] S. Hatscher, Schizophyllan as a Biopolymer for EOR Lab and Field Results, Winterfall, International Energy Agency (IEA), Germany, 2016.

View publication stats

DrEngMuslim - Karya Ilmiah - Comparing Natural And Synthetic Polymeric Nanofluids In A Mid-Permeability Sandstone Reservoir Condition

ORIGINALITY REPORT

17%	13%	13%	2%
SIMILARITY INDEX	INTERNET SOURCES	PUBLICATIONS	STUDENT PAPERS

MATCH ALL SOURCES (ONLY SELECTED SOURCE PRINTED)

10%

★ www.researchgate.net

Internet Source

Exclude quotes	On	Exclude matches	< 1%
Exclude bibliography	On		